Supporting Information

Fellin et al. 10.1073/pnas.0906419106

SI Materials and Methods

EEG/EMG Analysis. Stage scoring of computerized EEG/EMG epochs as rapid eye movement (REM), non-NREM, and wake was done in 4-s epochs by a trained experimenter blind to genotype using SleepSign (Kissei Comtec America). Spectral analysis was performed using a Fast Fourier Transform (FFT; Hanning Window). Frequency bins presented in Fig. 1 were normalized to the total power of the NREM EEG measured as the sum of the power bins between 0.39 and 20 Hz. Power of the slow oscillations (Fig. 1*B*) was computed by averaging the bins of the normalized power spectrum between 0.4 and 1 Hz. Late sleep (the last sleep episode of the light phase) was classified as a low homeostatic sleep pressure period (low pressure, Fig. 1), early sleep (the first sleep episode of the light phase) was classified as intermediate homeostatic sleep pressure period (intermediate pressure, Fig. 1). The third hour of recovery sleep after 6 h of sleep deprivation at the beginning of the light phase was classified as a high homeostatic sleep pressure period, and was chosen because our earlier studies (1), have shown it to be a time at which the difference between WT and dominant negative (dn)SNARE in slow wave activity (SWA) was maximal. Sleep deprivation was achieved by gentle handling.

In Vivo Patch-Clamp Recordings. Artificial cerebrospinal fluid (aCSF) on top of the craniotomy was removed before electrode insertion, and to identify when the pipette tip touched the cortical surface, the current flowing through the pipette after a 5 mV voltage step was monitored in voltage clamp. Once the electrode touched the brain, aCSF was rapidly added back on the cortical surface. The electrode was quickly lowered in the cortex for 50–100 μm to reach layer 2/3, and the positive pressure applied to the pipette was reduced approximately by one tenth. The electrode was then advanced in short steps (1–2 μm) while monitoring pipette resistance. A "hit" between the pipette tip and a cell membrane was identified by the rapid increase in pipette resistance and the appearance of heart beat frequency in the current trace. When a putative hit was observed, the positive pressure was released, and a negative pressure was applied to the pipette by gentle suction to obtain the gigaohm seal. After the whole-cell configuration was achieved, cells were recorded continuously in current clamp mode. Current pulses were applied at the beginning of the recording to monitor the pattern of the cell action potential discharge. Neuronal depolarizations (up-states) were defined as periods in which membrane voltage crosses a threshold (3× the half peak-to-peak noise of the trace) and stays above the threshold for >100 ms. The probability of the neuron being depolarized (up-state probability) was calculated by integrating membrane voltage over 30-s windows and dividing this value by the duration of the time window and the maximal amplitude of the up-state. Up-state probability and frequency were calculated every 2 min throughout the entire duration of the experiment. Values were then averaged to obtain a single value of up-state probability and frequency for each cell. The first 6 min since the beginning of the recording were not considered for analysis of up-state probability and frequency to allow dialysis of the pipette solution in the cell. When multiple cells where recorded from one animal, values from each cell were averaged together to obtain a single value for that specific animal. For the calculation of up- and down-state durations, membrane voltage traces were first leak subtracted to eliminate slow drift in the baseline and then idealized based on a threshold set at three times the half peak-to-peak noise amplitude of that particular recording. A transition from below to above the threshold that lasted for >100 ms was considered an up-state. Similarly, a transition from above to below the threshold that lasted for >200 ms was considered a down-state. Trace idealization and up- and down-state duration calculation were performed with TAC and TACFIT (Bruxton Corporation). To control for nonspecific effects of transgene expression, mice were maintained on a diet containing doxycycline (dox) to prevent transgene expression (2) during development. After the third week, postnatal dox was removed from the diet of animals. WT and bigenic dnSNARE mice received the same diet of dox.

Analysis of in Vivo Extracellular Recordings. For LFP analysis data were resampled at 1 KHz and low-pass filtered at 100 Hz. Power spectra were obtained by averaging a rectangular window (8,192 points) over a time period of 5–10 min, unless otherwise stated. For pharmacological experiments, power spectra after a given compound was applied were calculated after 20 min since drug application on the surface of the cortex, unless otherwise stated. Power spectra were normalized by the total power value obtained by integrating the whole power spectrum over frequency. Slow oscillation power was calculated by integrating the power spectrum between 0.36 to 1.09 Hz (slow oscillation range, 0.4–1 Hz) and normalized by the total power. For quantification of dye diffusion (Fig. S6 *C–E*), color images were converted into black and white, and pixel intensity along two different directions (90 and 45° from the plane tangential to the surface) was first background subtracted and then normalized to the average pixel intensity of a region close to the surface of the craniotomy, and finally, plotted as a function of the distance from the surface of the cortex. Dye diffusion was calculated in each animal as the distance at which dye intensity is half of its maximal value.

Slice Electrophysiology. Transverse brain slices (300 μm) were cut from 6- to 12-week-old animals. Experiments shown in Fig. S4 *A–E* were performed using 4- to 8-week-old mice. Cutting solution was as follows (in mM): NaCl 120, KCl 3.2, NaH_2PO_4 1, $NaHCO_3$ 26, $MgCl_2$ 2, $CaCl_2$ 1, glucose 2.8, Na-pyruvate 2 and ascorbic acid 0.6 at pH 7.4 with O_2 95%, CO_2 5%. After a recovery period of 50–60 min at 37 °C, slices were continuously perfused with the following recording solution (in mM): NaCl 120, KCl 3.2, NaH_2PO_4 1, $NaHCO_3$ 26, $MgCl_2$ 1, $CaCl_2$ 2, glucose 2.8, at pH 7.4 with O_2 95%, CO_2 5%. Patch-clamp recordings were performed at 30–35 °C. Glass electrode resistance was 3–4 MΩ. For AMPA/NMDA ratio measurements, intrapipette solution was (in mM): CsCl 140, NaCl 8, Na_2ATP 2, NaGTP 0.5, Hepes 10, Phophocreatine 10, QX-314 2.5 to pH 7.2 with CsOH. Biocytin (2 mg/mL) or neurobiotin (3 mg/mL) were included in the pipette solution for subsequent staining. For astrocyte recordings, intrapipette solution was the same used for in vivo experiments. Access resistance was not compensated and monitored throughout the entire duration of the experiment. Junction potentials were −18 mV, −15 mV, and −2.5 for in vivo recordings, astrocytes slice electrophysiology and AMPA/NMDA ratio measurements, respectively. Membrane potential values are not corrected for junction potentials. Signals were filtered at 1 KHz and digitized at 5 KHz. For AMPA/NMDA ratio measurements (3), layer 2/3 neurons were recorded while stimulating layer 4 at 0.1 Hz with an extracellular electrode (FHC). The $GABA_A$ receptor antagonist picrotoxin (100 μM) was always added to the recording solution while measuring AMPA/NMDA ratio. After a stable EPSC was obtained, AMPA

currents were first recorded at −70 mV, then the AMPA receptor antagonist 2,3-Dioxo-6-nitro-1,2,3,4-tetrahydrobenzo quinoxaline -7-sulfonamide (NBQX; 10 μM) was added to the solution and finally NMDA currents were measured at +40 mV. EPSC amplitude was measured at the peak. Peak values were corrected for current rundown during the experiment.

Immunohistochemistry. Mice were cardiac perfused with cold PBS and then with paraformaldehyde (4% in PBS). The brain was extracted, postfixed in paraformadehyde, transferred overnight in 30% sucrose, and finally, frozen and stored at −80 °C. Coronal sections (40 μm) were cut, subsequently washed with PBS three times, and permeabilized with 1% BSA (Vector Labs), 0.1% Triton X-100, 5% horse or goat serum in PBS. Unless otherwise indicated, the antibodies used were from Millipore. We used mouse NeuN antibody, 1:1,000, rabbit polyclonal ASPA (kind gift from James Garbern, Wayne State University School of Medicine, Detroit, MI), 1:1,000, rabbit NG2 antibody, 1:1,000, rabbit GFAP antibody (Sigma), 1:1,000, rabbit Iba1 antibody (Wako Chemicals), 1:500, Rabbit anti-glutamate receptor 1 antibody (1:1,000), and Anti-NR2A (1:1,000). For ASPA staining, tissues were previously permeabilized with Methanol for 30 min at −20 °C. After washing in 2% Normal serum, 0.3% Triton X-100, 1X PBS, sections were incubated for 2 h at room temperature with the appropriate secondary antibodies conjugated to Alexa Fluor 546 (Invitrogen). Sections were then mounted on slides and analyzed on a confocal microscope (Olympus). For morphological reconstruction, neurons were filled with biocytin or neurobiotin during the recording. After fixation, sections were then incubated with streptavidin Alexa Fluor 546 or streptavidin Texas Red for 4 h at room temperature. After washing in PBS, sections were mounted on coverslip, and images were taken with an Olympus Fluoview 1000 confocal microscope. The same procedures described above were used for biotin staining of neurons recorded in situ after slice fixation in paraformaldehyde.

Western Blotting. Slices from the somatosensory cortical region were incubated in ACSF at 32 °C for at least 1-h recovery before experimentation. Slices were then placed on ice and incubated for 30 min with 1 mg/mL NHS-SS-biotin (Pierce). Excess biotin was removed by washing 3 times in cold ACSF and homogenized in a buffer containing 20 mM Tris·HCl, pH 8.0, 150 mM NaCl, 5 mM EDTA, 1% Triton X-100, 0.1% SDS, 10 mM NaF, 2 mM Na_3VO_4, 10 mM $Na_4P_2O_7$, 10 μg/mL leupeptin, 1 μg/mL aprotinin, 10 μg/mL antipain and 250 μg/mL 4-(2-Aminoethl) benzenesulfonyl fluoride hydrochloride. Insoluble material was removed by centrifugation, and lysates were incubated with Streptavidin beads (Pierce) for 12 h at 4 °C (4, 5). Bound material was subjected to SDS/PAGE and then immunoblotted with NMDAR (NR2B, BD Transduction Laboratories; NR2A: Upstate, NR1, BD PharMingen), AMPAR (GluR1, Chemicon; GluR2, Abcam), β-Actin (Sigma), EAAT2 (kind gift from Michael Robinson, University of Pennsylvania, Philadelphia, PA), and α-Tubulin (Sigma) antibodies and visualized by ECL (Pierce). Blots were then quantified using the CCD based FujiFilm LAS 3000 system.

1. Halassa MM, et al. (2009) Astrocytic adenosine controls sleep homeostasis and cognitive consequences of sleep loss. *Neuron* 61:213–219.
2. Pascual O, et al. (2005) Astrocytic purinergic signaling coordinates synaptic networks. *Science* 310:113–116.
3. Panatier A, et al. (2006) Glia-derived D-serine controls NMDA receptor activity and synaptic memory. *Cell* 125:775–784.
4. Terunuma M, et al. (2008) Deficits in phosphorylation of GABA(A) receptors by intimately associated protein kinase C activity underlie compromised synaptic inhibition during status epilepticus. *J Neurosci* 28:376–384.
5. Saliba RS, Michels G, Jacob TC, Pangalos M, Moss SJ (2007) Activity-dependent ubiquitination of GABA(A) receptors regulates their accumulation at synaptic sites. *J Neurosci* 27:13341–13351.

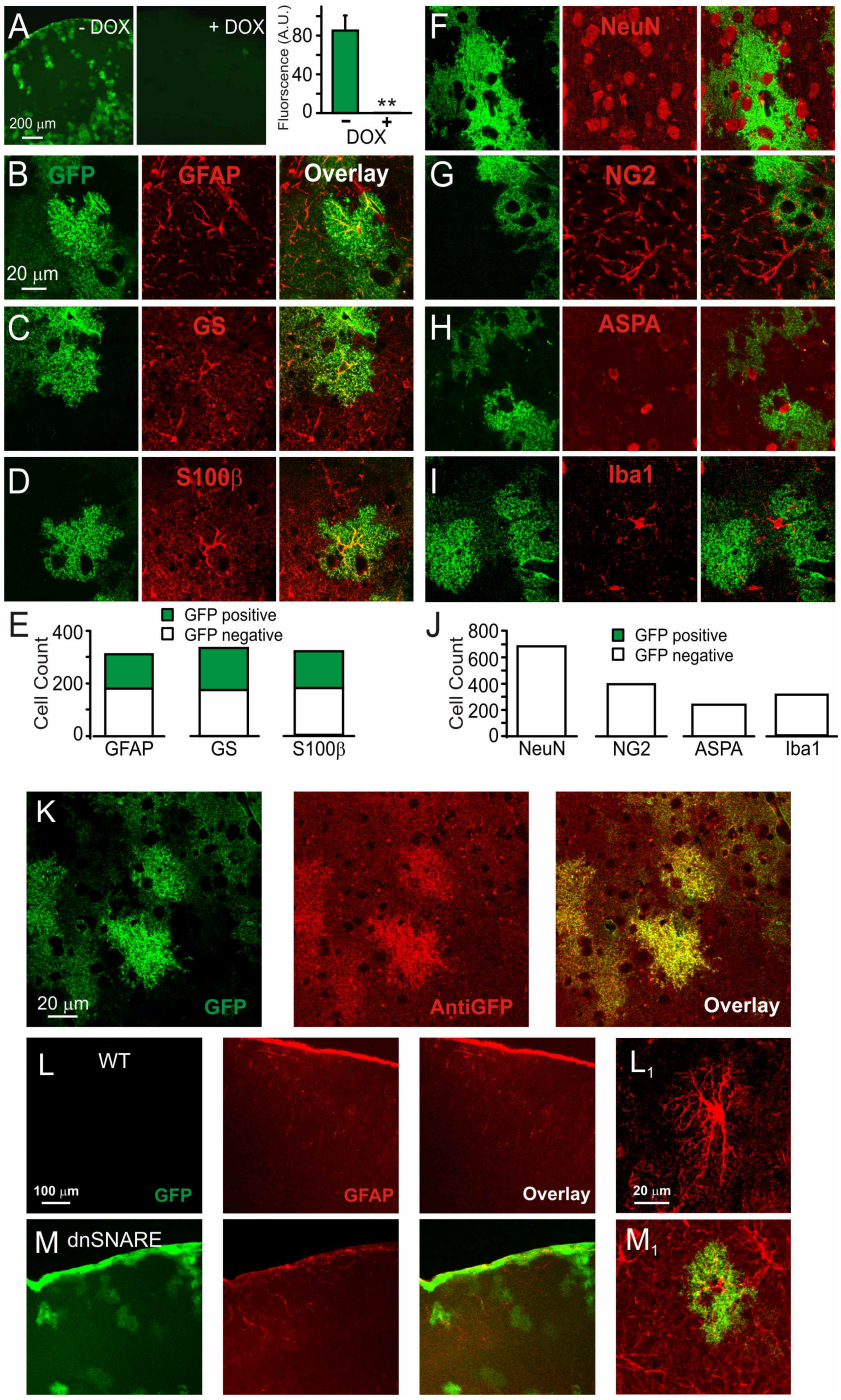

Fig. S1. Dominant negative SNARE transgenes are selectively expressed in cortical astrocytes in the absence of dox. (*A*) Confocal image showing expression of the reporter transgene EGFP (green) throughout the different layers of the cortex in the absence (− DOX) and in the presence (+ DOX) of dox. Mice were raised on dox until the third week postnatal and then dox was either removed (− DOX) or maintained (+ DOX) in the food for at least three additional weeks. Experiments with mice − and + DOX were performed in parallel, and same settings of the confocal microscope were used for image acquisition. (*Right*) Quantification of transgene expression obtained by measuring the intensity of the EGFP fluorescence. Note that, in the presence of dox, EGFP fluorescence is drastically reduced, confirming that transgene expression is negligible when mice are fed dox. (*B–D*) Single plane confocal images showing colocalization (*Right*) between the reporter transgene EGFP (GFP, green; *Left*) and the astrocytic marker GFAP (red, *B Middle*), glutamine synthase (GS, *C*) and S100β (*D*). (*E*) Quantification of the overlay between the reporter transgene EGFP and the astrocytic markers GFAP, GS, and S100 β. (*F–I*) EGFP does not colocalize with NeuN (*F*), NG2 (*G*), aspartocyclase (ASPA) (*H*), and Iba1 (*I*), markers of neurons, NG2-positive cells, oligondendrocytes, and microglia. (*J*) Quantification of the overlay between EGFP and NeuN (*F*), NG2 (*G*), ASPA (*H*), and Iba1 (*I*). Data in this figure were collected from multiple sections from at least three different animals. (*K*) Confocal images showing native fluorescence of EGFP (GFP, green; *Left*) and immunostaining against GFP (red; *Middle*) in dnSNARE animals. Overlay is shown in *Right*. (*L* and *M*) GFAP staining shows similar immunoreactivity in WT (*L*) and dnSNARE (*M*) animals. Images at higher magnification are shown in L_1 and M_1 for WT and dnSNARE animals, respectively.

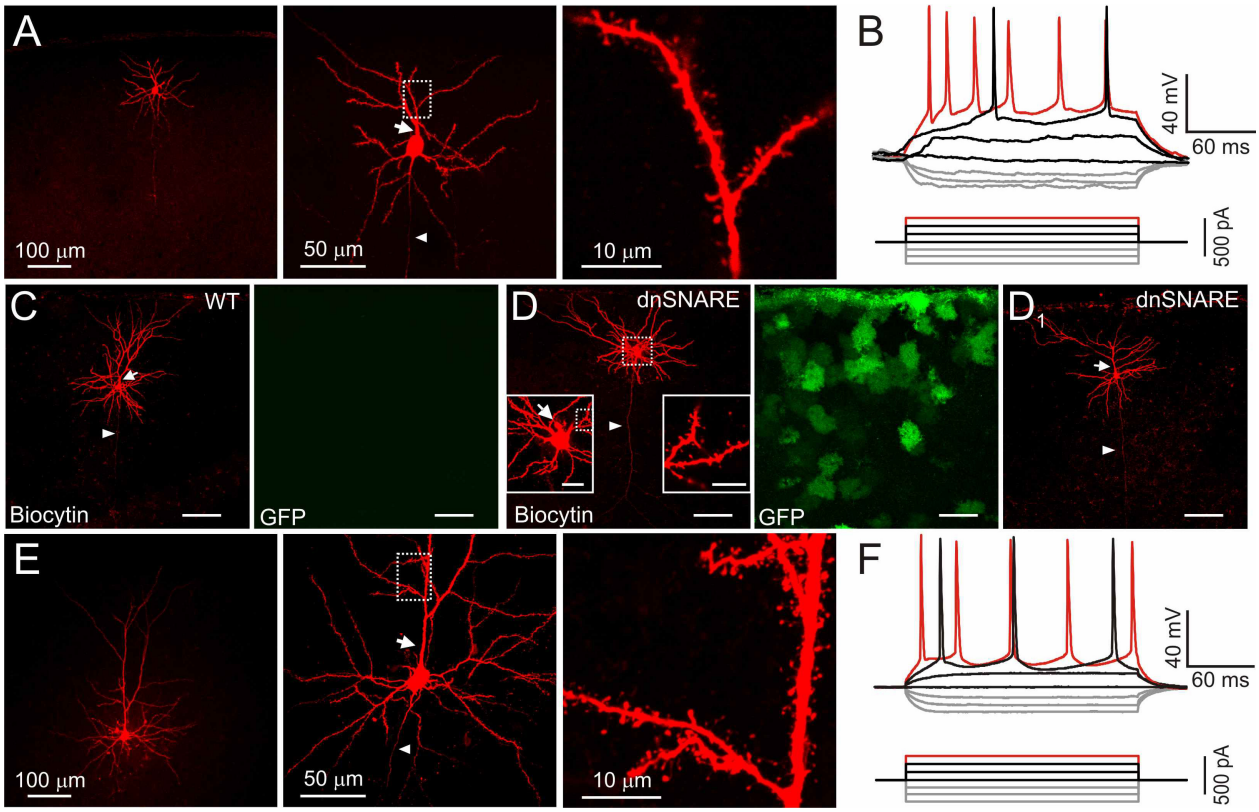

Fig. S2. Morphological and electrophysiological identification of recorded neurons. (*A*) Z-projection of a confocal z-stack showing a biocytin-filled neuron in vivo at different levels of magnification. All recorded cells display the typical feature of pyramidal cells, i.e., a clear apical dendrite (arrow in *Middle*), a large cell somata, elaborate dendritic arborization within and across the cortical layers, a descending axon (arrowhead), and a high density of dendritic spines (*Right*). The three images are z-projections of a different number of confocal planes. (*B*) Cell identification was confirmed by injecting current pulses and observing the firing properties. Cells display regular firing properties showing some degree of accomodation and increasing spike frequency as a function of the injected current. (*C* and *D*) The z-projection of confocal z-stacks showing biotin staining (red) of neurons (recorded in Fig. 3) from the somatosensory cortex of WT and transgenic animals. Transgenic, but not WT sections display fluorescence of the reporter transgene EGFP (GFP, green) in cortical astrocytes. Note that the recorded neurons display the characteristic features of pyramidal cells: a clear apical dendrite (arrow), large horizontal arborization, a descending axon (arrowhead), and a high density of dendritic spines (*D Inset*). The apical dendrite of the cell displayed in *D* was probably cut during the slice preparation, and thus, only the initial part is visible (arrow in *Inset*). (*D*1) Additional example of layer 2/3 pyramidal neuron recorded in slice from the dnSNARE animal. [Scale bars, 100 μm. (*D Inset*); 20 μm (*Left*); 10 μm (*Right*).] (*E*) Same as in *A* for a cortical neuron recorded in slice preparation. (*F*) Injection of current pulses in the cell displayed in *E* shows regular firing properties typical of pyramidal cells.

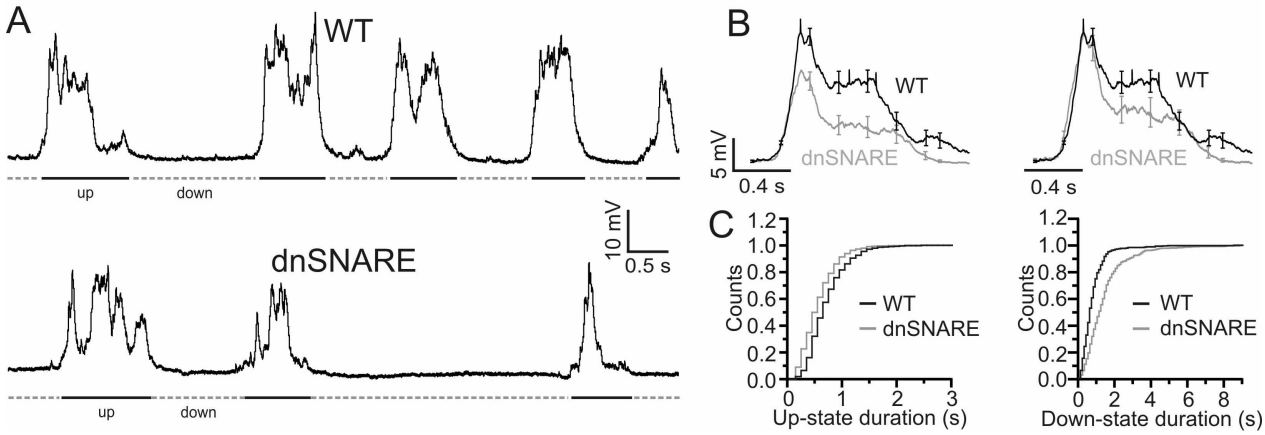

Fig. S3. Shorter up- and longer down-state durations in dnSNARE animals. (*A*) Representative example of up- (continuous black line) and down-state (dotted gray line) transitions obtained from patch-clamp recordings in vivo shown in Fig. 2 from WT and dnSNARE animals at an expanded time scale. (*B*) Average of a series ($>$ 20) of consecutive up-states from a WT (black trace) and dnSNARE (gray trace). Traces are shown normalized to their maximum value on the right. (*C*) Cumulative distributions of up- (*Left*) and down-state (*Right*) durations for WT (black) and dnSNARE (gray). Data are obtained from 11 cells from 8 WT and 14 cells from 9 dnSNARE animals.

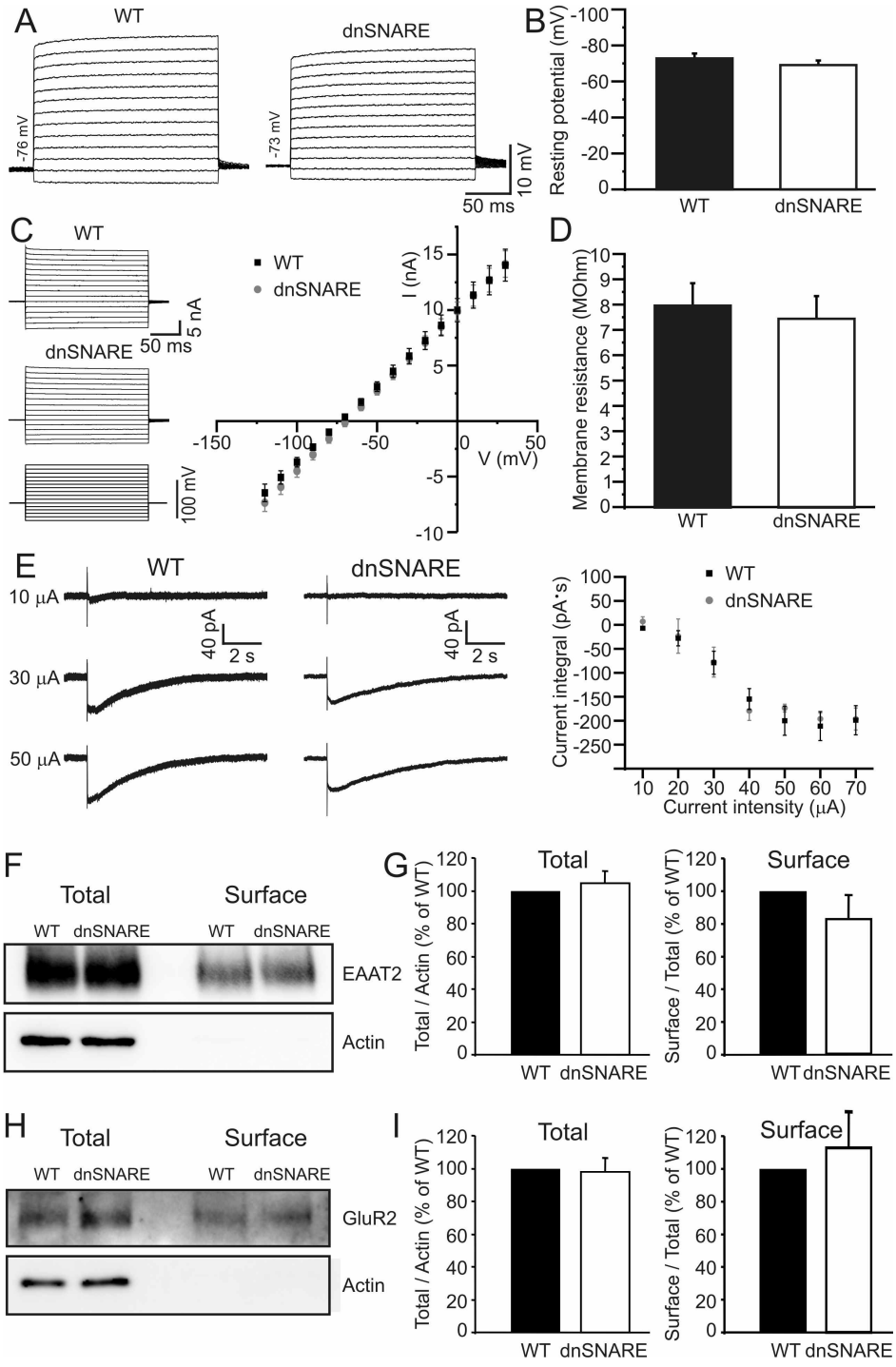

Fig. S4. Dominant negative SNARE expression does not affect astrocytic supportive functions. (*A* and *B*) Examples of current clamp recordings from hippocampal astrocytes from WT and dnSNARE animals (*A*) and average astrocytic resting potentials ($P > 0.05$) (*B*). Data are obtained from nine cells from three WT and seven cells from three dnSNARE animals. (*C*) Average whole-cell I-V relationship from nine WT and seven dnSNARE cells showing typical passive properties of both WT and dnSNARE astrocytes. (*Inset*) Representative current responses from a WT (*Top*) and dnSNARE (*Bottom*) astrocytes. (*D*) Average input resistance is not significantly different between WT ($n = 9$) and dnSNARE ($n = 7$, $P > 0.05$). (*E*) (*Left*) Representative current response of astrocytes to stimulation of the Schaffer collateral pathway with different stimulation intensities. A quantification of the experiments shown in *Left* is obtained by calculating the total charge passing through the astrocytic membrane obtained by integrating the current trace over time. Average data from 6 cells from 3 WT and 3 cells from 2 dnSNARE animals are shown. (*F*) Total (*Left*) and cell surface (*Right*) protein in cortical slices of WT and dnSNARE animals was blotted with anti-EAAT2 and β-actin antibodies. (*G*) Average of total (*Left*) and surface (*Right*) expression of the glutamate transporter EAAT2. Total, $P = 0.29$; surface $P = 0.16$, $n = 4–5$. (*H* and *I*) Same as in *F* and *G* for the GluR2 subunit. (*I*) Total, $P = 0.41$; surface $P = 0.31$, $n = 4$.

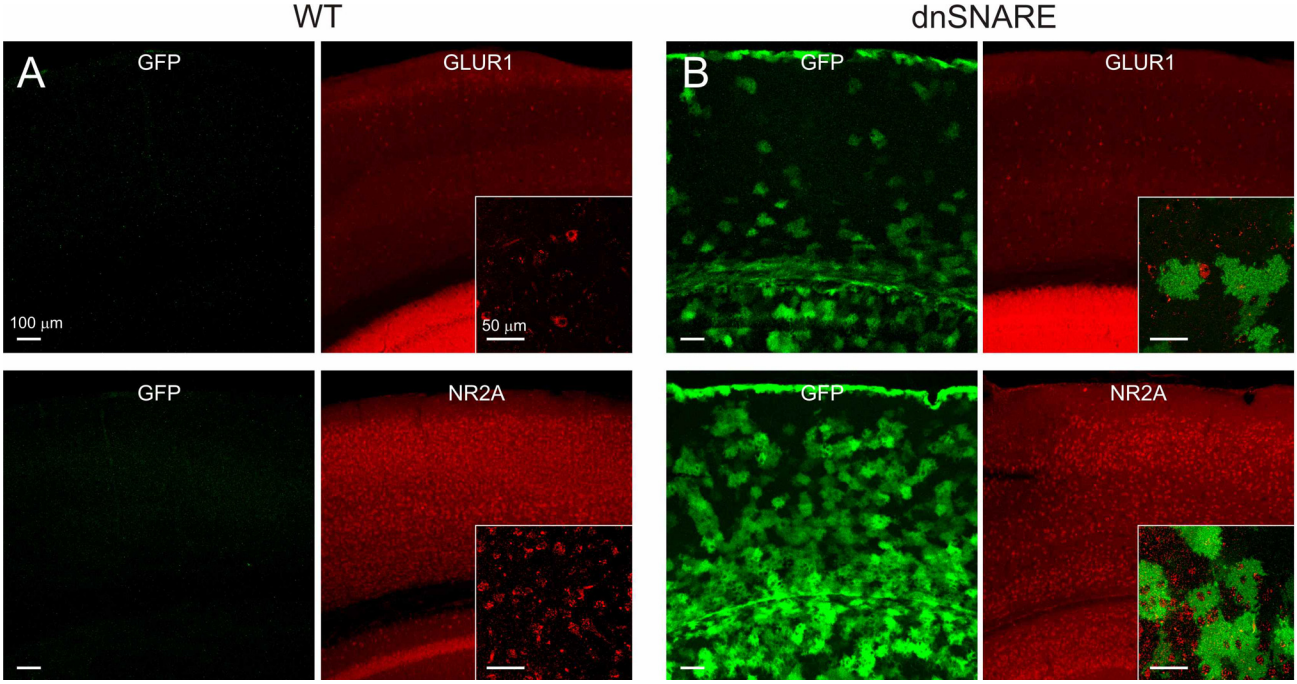

Fig. S5. Similar immunoreactivity of AMPA and NMDA receptors in WT and dnSNARE animals. (*A*) The z-projections of confocal z-series showing immunostaining against the GluR1 (red; *Top*) and NR2A (red; *Bottom*) subunits of the AMPA and NMDA receptors respectively. (*Left*) Lack of EGFP signal (GFP) in WT animals. (*B*) Same as in *A* for the dnSNARE animals.

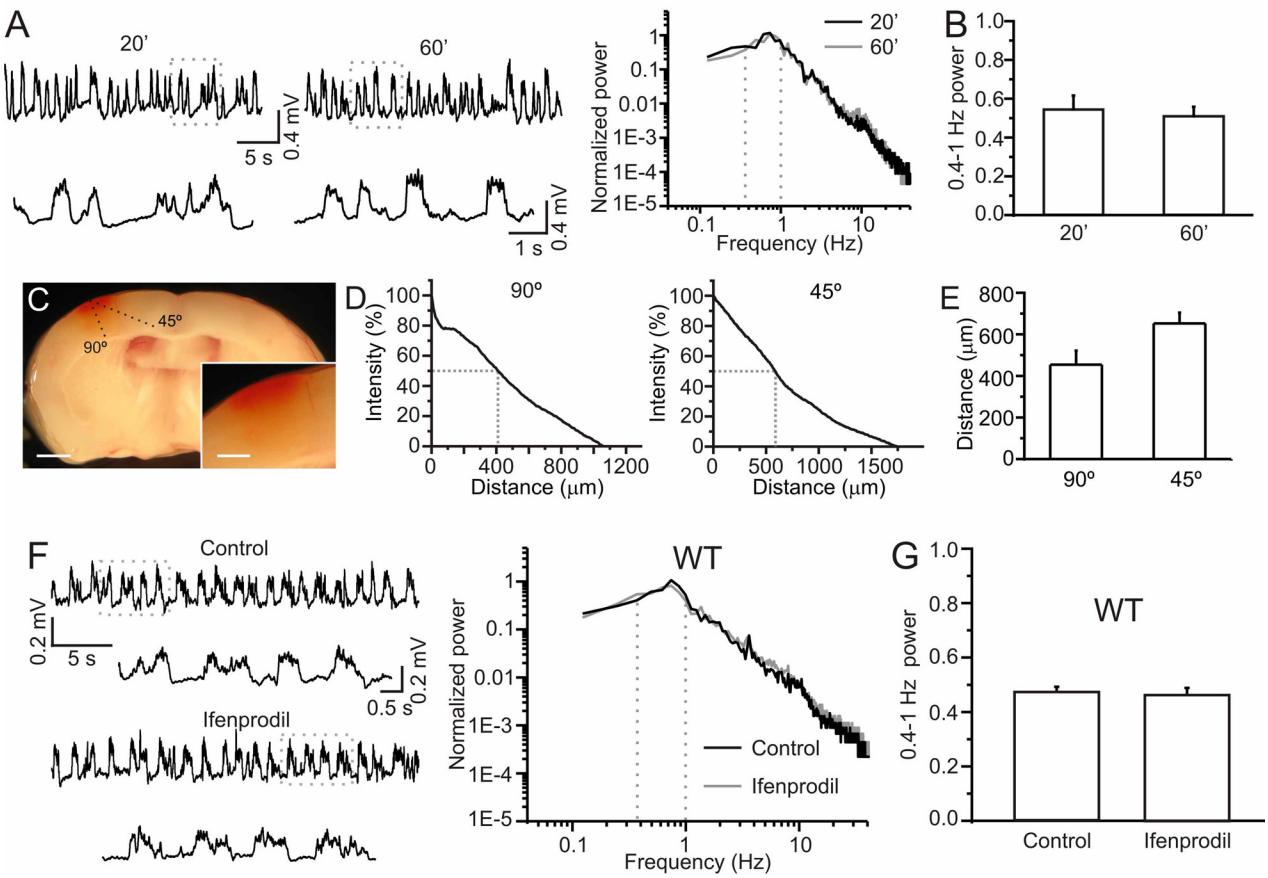

Fig. S6. Stability of slow oscillation activity and drug diffusion through cortical layers. (*A*) Traces (*Left*) and power spectra (*Right*) of LFP signals after 20 and 60 min from the beginning of the experiment. Power spectra were calculated in a 2-min time window. (*B*) Average power of the slow oscillations after 20 and 60 min from the beginning of the experiment in 7 different animals. $P > 0.05$. (*C*) Image showing dye diffusion through cortical layers after 30 min of application of phenol red (10 mM) on the brain surface. (*D*) Dye concentration as a function of the distance from the surface of the cortex. Dye concentration (see *Materials and Methods*) was calculated along a direction perpendicular to the surface (90°) and at 45°. [Scale bars, 1 mm; 500 μm (*Inset*).] (*E*) Average values of dye diffusion, measured as the distance at which dye intensity is half of its maximal value ($n = 6$ animals). (*F*) Traces (*Left*) and power spectra (*Right*) of LFP signals before and after ifenprodil (10–15 μM) application. (*G*) Average power of the slow oscillations under the different experimental conditions in 6 different animals. $P > 0.05$.

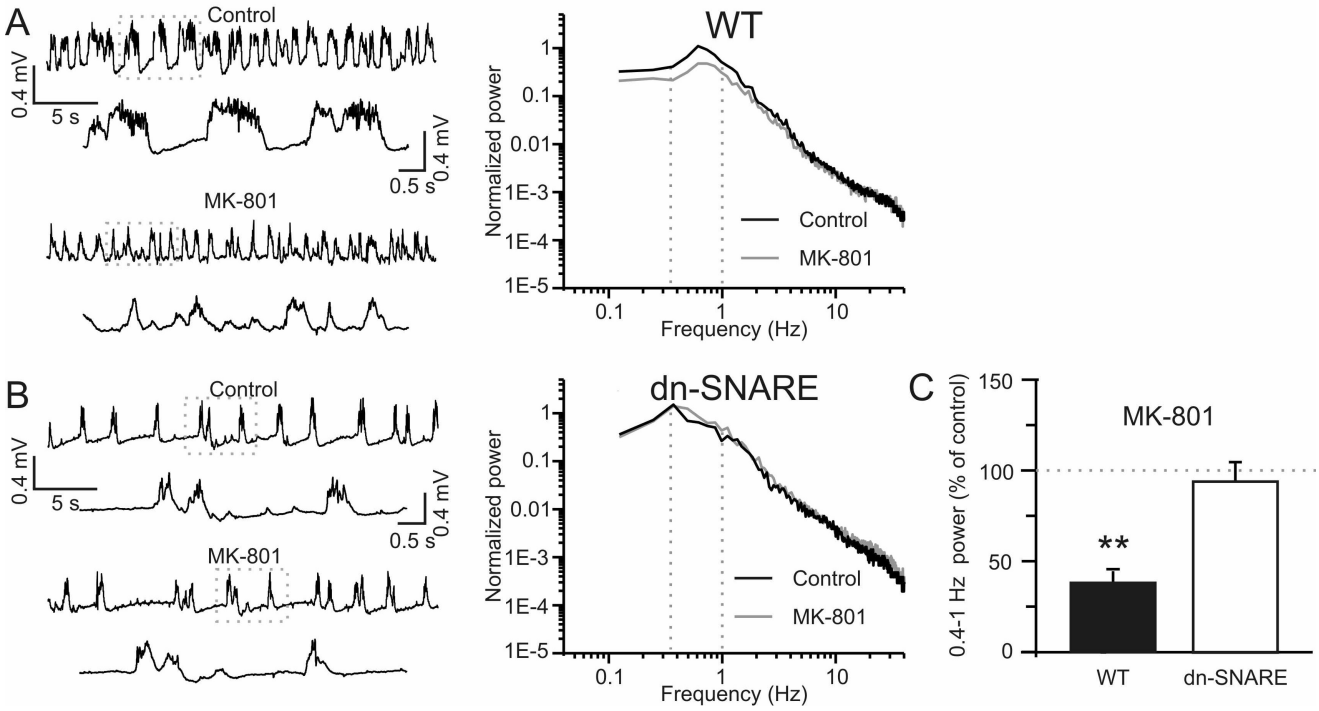

Fig. S7. A different NMDA receptor antagonist, MK-801, reduces the power of cortical slow oscillations in WT, but not dnSNARE animals. (*A* and *B*) Example of LFP traces and power spectra of a WT (*A*) and dnSNARE (*B*) under control conditions and after application of MK-801 (20 μM). (*C*) Average decrease in slow oscillation power after MK-801 application (20–40 μM; WT, $n = 6$ animals; dnSNARE, $n = 6$ animals).

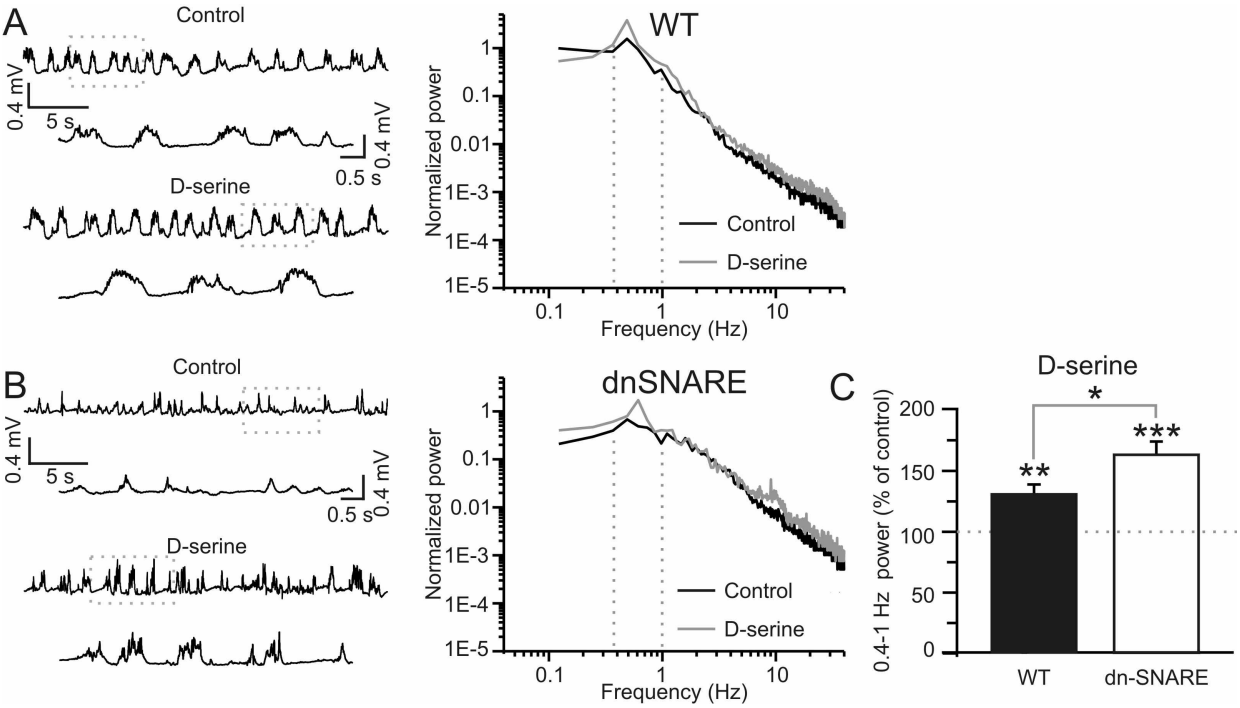

Fig. S8. Application of exogenous D-serine increases slow oscillations. (*A* and *B*) Representative LFP recording and corresponding power spectra of a WT (*A*) and a dnSNARE (*B*) animal under control conditions and after application of exogenous D-serine (300 μM). Power spectra after pharmacological application are taken between the 15th and 20th minute after drug application. (*C*) Average slow oscillation power before and after D-serine application (300 μM; WT, **, $P < 0.01$, $n = 10$ animals; dnSNARE, ***, $P < 0.001$, $n = 9$ animals, *, $P < 0.05$).

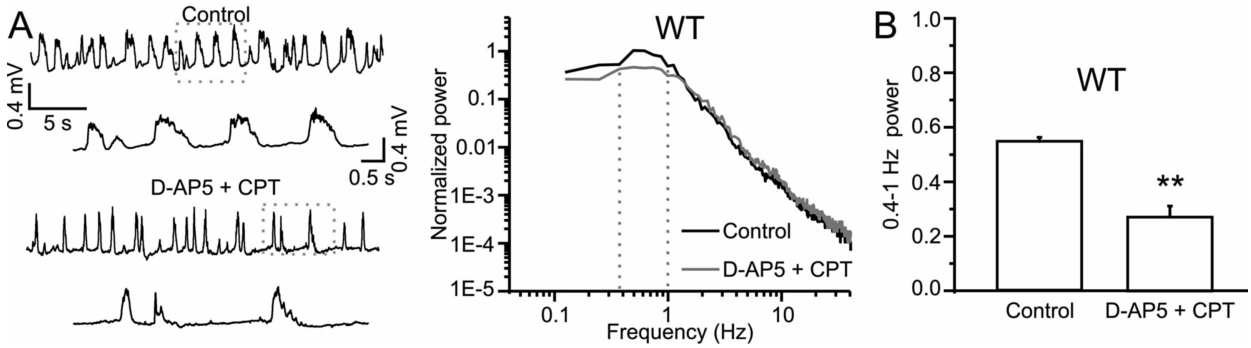

Fig. S9. Block of NMDA and A1 receptors in WT animals leads to an overall decrease in the power of the slow oscillations. (*A*) Traces (*Left*) and power spectra (*Right*) showing the effect of the coapplication of the NMDA receptor antagonist D-AP5 (50–100 μM) and CPT (1 μM) on slow oscillation activity in WT mice. (*B*) Mean values of slow oscillation power under control conditions and after D-AP5 and CPT application ($n = 5$).

Table S1. Dominant negative SNARE expression in astrocytes does not affect neuronal membrane properties

	Resting potential, mV	Input resistance, MΩ	*N*
WT	−62.2 ± 1.5	151.6 ± 12.4	8
dnSNARE	−60.5 ± 1.3	132.5 ± 22.8	9

Resting membrane potential and input resistance of 11 neurons recorded from eight WT and 15 neurons from nine dnSNARE animals. When multiple cells were recorded from one animal, values were averaged together to get one number representative of that single animal. Note that values are not corrected for liquid junction potential (see *Materials and Methods*). $P > 0.4$.